Available online at www.sciencedirect.com
ScienceDirect
Journal of Computational Physics 227 (2007) 851–870
JOURNAL OF COMPUTATIONAL PHYSICS
www.elsevier.com/locate/jcp

Explicit time-domain approaches based on numerical Green's functions computed by finite differences – The ExGA family

W.J. Mansur *, F.S. Loureiro, D. Soares Jr., C. Dors

Department of Civil Engineering, COPPE/Federal University of Rio de Janeiro, CP 68506, CEP 21945-970, Rio de Janeiro, RJ, Brazil

Received 2 October 2006; received in revised form 3 August 2007; accepted 31 August 2007
Available online 7 September 2007

Abstract

The present paper describes a new family of time stepping methods to integrate dynamic equations of motion. The scalar wave equation is considered here; however, the method can be applied to time-domain analyses of other hyperbolic (e.g., elastodynamics) or parabolic (e.g., transient diffusion) problems. The algorithms presented require the knowledge of the Green's function of mechanical systems in nodal coordinates. The finite difference method is used here to compute numerically the problem Green's function; however, any other numerical method can be employed, e.g., finite elements, finite volumes, etc. The Green's matrix and its time derivative are computed explicitly through the range $[0, \Delta t]$ with either the fourth-order Runge–Kutta algorithm or the central difference scheme. In order to improve the stability of the algorithm based on central differences, an additional matrix called step response is also calculated. The new methods become more stable and accurate when a sub-stepping procedure is adopted to obtain the Green's and step response matrices and their time derivatives at the end of the time step. Three numerical examples are presented to illustrate the high precision of the present approach.

Keywords: Explicit Green approach; Transient dynamics; Scalar wave equation; Time integration; Numerical Green's function; Sub-steps

1. Introduction

Time dependent partial differential equations have numerous applications in various branches of science and in practical engineering design. Since it is usually very difficult to obtain transient responses analytically for these equations, numerical techniques must be used to find approximate solutions.

Step-by-step time integration algorithms are routinely used when hyperbolic differential equations, such as the wave equation considered here, need to be solved, because of their various inherent advantages to solve a great deal of initial value problems.

* Corresponding author. Tel.: +55 21 2562 7382.
E-mail address: webe@coc.ufrj.br (W.J. Mansur).

0021-9991/$ - see front matter
doi:10.1016/j.jcp.2007.08.024

The literature reports many classical explicit [1–6] and implicit [7–11] algorithms for time marching; for a comprehensive review see [12]. Explicit procedures are preferable because they are cheaper and faster, restrictions due to stability conditions being their main weakness. Many procedures can be employed to improve stability and accuracy of time-integration algorithms, e.g., subcycling techniques [13–15], high-order accurate schemes [16–21] and automatic time step control [22].

The family of algorithms presented here deals with time integration of the equations of motion by the association of standard explicit schemes with the corresponding time-domain boundary integral equation [23] through the solution based on explicit determination of numerical Green's functions (ExGA family). It is worth mentioning that the term "explicit" is employed in the sense that the Green's functions are explicitly computed.

Wrobel [24] developed a time-stepping algorithm based on analytical expressions of Green's functions of homogeneous infinite media and Soares and Mansur [25] developed a formulation that uses Green's functions implicitly within standard time-marching schemes. Tamma et al. [26] and Zhou and Tamma [27] derived a new family of unconditionally explicit or implicit algorithms based on analytical solution of first-order ordinary differential equations in which the concept of Green's functions is also implicitly present.

The time-domain boundary integral equation presented by Mansur [23] can be used as a starting point for the developments presented here. In the procedure discussed in the present paper the major limitation of BEM approaches is removed, i.e., it is not necessary to have an analytical expression for the Green's function of the problem, rather, it is computed numerically. Any standard numerical method can be employed to compute the problem Green's function, thus, there is no limitation at all, i.e., the medium can be non-homogeneous, anisotropic, viscoelastic, poroelastic, etc. The price to pay for the aforementioned generality is the discretization of the domain; however, substantial accuracy and stability improvements are achieved. In fact if sub-steps are employed, it is possible to choose the maximum time step for which explicit Green's function based algorithms are stable and accurate. One can easily employ time steps thousands times larger than those permitted by the central difference or Runge–Kutta methods; the only restriction on the time-step "length" being now concerned with having a good picture of the time response history.

Two Green's function explicit approaches, applied to the scalar wave equation, are considered in the present paper:

(i) ExGA – In this approach the Green's function (**G** matrix) and its time derivative ($\dot{\mathbf{G}}$ matrix) transfer, respectively, initial velocity and initial displacement, both weighted by mass, from 0 to Δt. If viscous damping is considered, an additional effect proportional to the product of the initial displacement vector times the viscous matrix is transferred from 0 to Δt by the problem Green's function.
(ii) ExGAH – In this approach, initial velocity effects are transferred from 0 to Δt as in the previously described one. The effects of initial displacements are transferred from 0 to $\Delta\ t$ by the so called step response matrix (**H**), which stores responses at Δt, due to individual spatial distribution of initial displacements represented by nodal interpolation functions (if the FEM is employed, or equivalent approaches for other methods) and computes the response at Δt by superposition, as given by the product $\mathbf{HU}(0)$.

The two approaches are equivalent, their difference being the matrices employed to compute initial displacements effects. The ExGA approach is entirely new; a preliminary version can be found in [28,29]. The basic concepts leading to it can be found in [23,25], the former presents the version on integral representations and the latter presents the implicit version.

Approaches similar to the ExGAH have been the subject of some papers discussion, and are usually referred to as "precise time-step integration methods", as can be seen in [30,31,13]. The interpretation of the step response matrix as a matrix that transfers the contributions of $\mathbf{U}(0)$ to $\mathbf{U}(\Delta t)$ via superposition in space of contributions of individual nodes can be easily inferred from Eq. (9) of the present paper.

It is shown here that one can compute **G**, **H** and $\dot{\mathbf{G}}$ matrices employing any numerical approach to discretize in time and space. The discussion presented here shows that arbitrary time-steps subdivisions can be employed to compute **G**, $\dot{\mathbf{G}}$ and **H** matrices, and introduces a general scheme to compute convolution integrals which account for nodal loads contributions even when sub-steps are employed.

The Green's function **G**, the step response function **H**, and their time derivatives are computed using finite differences discretization in space and either central differences or fourth-order Runge–Kutta for time

integration. The following notation distinguishes the combinations employed: ExGA(H) – b[a], where the Green's function matrix **G** and its time derivate $\dot{\mathbf{G}}$ (or matrices **G** and **H**) are computed employing a second ($a = 2$) or fourth ($a = 4$) order finite difference operator in space and central differences ($b = \mathrm{CD}$) or fourth-order Runge–Kutta ($b = \mathrm{RK}$) to march on time. Absence of superscripts means no spatial discretization, i.e., in the present paper it indicates a SDOF spring–mass–dashpot system.

2. Equations of motion

The dynamic equilibrium equation for scalar wave propagation problems reads

$$\nabla(K\nabla u(\mathbf{x},t)) - c\dot{u}(\mathbf{x},t) - \rho\ddot{u}(\mathbf{x},t) = f(\mathbf{x},t) \tag{1}$$

where K, c and ρ are the problem physical parameters, which in the present analysis are considered to be time independent. Eq. (1) can represent many different physical problems, e.g., acoustic wave propagation, SH wave propagation in elastic media, transverse motion of taught strings and membranes, etc.

When the finite element method (FEM) or the finite difference method (FDM) is applied, Eq. (1) can be written as [32–36]:

$$\mathbf{M}\ddot{\mathbf{U}}(t) + \mathbf{C}\dot{\mathbf{U}}(t) + \mathbf{K}\mathbf{U}(t) = \mathbf{F}(t) \tag{2}$$

If a structural system is being considered, **M**, **C** and **K** denote mass, damping and stiffness matrices, respectively, $\mathbf{F}(t)$ is the nodal equivalent load vector and $\ddot{\mathbf{U}}(t)$, $\dot{\mathbf{U}}(t)$ and $\mathbf{U}(t)$ are, respectively, unknown acceleration, velocity and displacement vectors. The solution of Eq. (2) can be obtained by a numerical step-by-step procedure with initial conditions at time $t = 0$ given by $\mathbf{U}(0)$ and $\dot{\mathbf{U}}(0)$.

Modal decomposition can be invoked to compute the solution of Eq. (2). In this case, uncoupled equations, as indicated below (one for each mode), have to be solved. Solution of Eq. (2) is then obtained by transforming results back from modal to physical coordinates.

$$\ddot{u}(t) + 2\xi\omega\dot{u}(t) + \omega^2 u(t) = f(t) \tag{3}$$

In Eq. (3), ω is the eigenfrequency corresponding to a particular vibration mode and ξ and $f(t)$ are, respectively, the damping ratio and the modal excitation force.

The modal displacement $u(t)$ in Eq. (2) can be calculated by the Duhamel integral [37–39], as

$$u(t) = (\dot{g}(t) + 2\xi\omega g(t))u(0) + g(t)\dot{u}(0) + \int_0^t g(t-\tau)f(\tau)\mathrm{d}\tau \tag{4}$$

where $u(0)$ and $\dot{u}(0)$ are initial conditions and $g(t)$ and $\dot{g}(t)$ are, respectively, the Green's function corresponding to Eq. (3) and its time derivative. The exact Green's functions for the single-degree-of-freedom mechanical system represented by Eq. (3) is given by [32–39]:

$$\begin{aligned} g(t) &= \exp(-\omega\xi t)\left(\frac{1}{\omega_\mathrm{d}}\sin(\omega_\mathrm{d}t)\right) \\ \dot{g}(t) &= \exp(-\omega\xi t)\left(\cos(\omega_\mathrm{d}t) - \frac{\omega\xi}{\omega_\mathrm{d}}\sin(\omega_\mathrm{d}t)\right) \end{aligned} \tag{5}$$

where $\omega_\mathrm{d} = \omega\sqrt{1-\xi^2}$ and for $t = 0$, one has $g(0) = 0$ and $\dot{g}(0) = 1$.

There are quite a few approaches in the literature with the exact amplification matrix in modal coordinates and others with approximations in the physical time space (not modal space), for a more comprehensive review, see [31,40–42].

3. The Explicit Green approach (ExGA)

The previous section showed the analytical solution of the second-order differential equation for a single-degree-of-freedom system. In this paper, Eq. (2) is manipulated directly, so that Eq. (4) can be back transformed to physical coordinates, giving (see [25,28,29,43]):

$$\mathbf{U}(t) = (\mathbf{G}(t)\mathbf{C} + \dot{\mathbf{G}}(t)\mathbf{M})\mathbf{U}(0) + \mathbf{G}(t)\mathbf{M}\dot{\mathbf{U}}(0) + \int_0^t \mathbf{G}(t-\tau)\mathbf{F}(\tau)\mathrm{d}\tau \tag{6}$$

The velocity, which is calculated by differentiating Eq. (6) with respect to time, is given by

$$\dot{\mathbf{U}}(t) = (\dot{\mathbf{G}}(t)\mathbf{C} + \ddot{\mathbf{G}}(t)\mathbf{M})\mathbf{U}(0) + \dot{\mathbf{G}}(t)\mathbf{M}\dot{\mathbf{U}}(0) + \int_0^t \dot{\mathbf{G}}(t-\tau)\mathbf{F}(\tau)\mathrm{d}\tau \tag{7}$$

In many engineering problems, analytical expressions for the Green's functions are not known, thus, the Green's matrix must be calculated numerically by a time integration method. Assuming that the time step is Δt, Eqs. (6) and (7) can be used to recursively evaluate displacement and velocity vectors at any time t as indicated below:

$$\begin{aligned}
\mathbf{U}^{t+\Delta t} &= (\mathbf{G}(\Delta t)\mathbf{C} + \dot{\mathbf{G}}(\Delta t)\mathbf{M})\mathbf{U}^t + \mathbf{G}(\Delta t)\mathbf{M}\dot{\mathbf{U}}^t + \int_t^{t+\Delta t} \mathbf{G}(t+\Delta t-\tau)\mathbf{F}(\tau)\mathrm{d}\tau \\
\dot{\mathbf{U}}^{t+\Delta t} &= (\dot{\mathbf{G}}(\Delta t)\mathbf{C} + \ddot{\mathbf{G}}(\Delta t)\mathbf{M})\mathbf{U}^t + \dot{\mathbf{G}}(\Delta t)\mathbf{M}\dot{\mathbf{U}}^t + \int_t^{t+\Delta t} \dot{\mathbf{G}}(t+\Delta t-\tau)\mathbf{F}(\tau)\mathrm{d}\tau
\end{aligned} \tag{8}$$

The following integral equation presented by Mansur [23], can be used to illustrate a classical procedure based on Green's function, which applies for undamped ($c = 0$) homogeneous media (time derivative of Eq. (9), which gives the expression for $\dot{u}(s,t)$, can be found in [44]):

$$\begin{aligned}
u(s,t) = \frac{1}{4\pi k}\Bigg\{ &\int_0^{t^+}\int_\Gamma u^*(Q,t;s,\tau)p(Q,\tau)\mathrm{d}\Gamma(Q)\mathrm{d}\tau - \int_0^{t^+}\int_\Gamma p^*(Q,t;s,\tau)u(Q,\tau)\mathrm{d}\Gamma(Q)\mathrm{d}\tau \\
&-\rho\int_\Omega v_0^*(q,t;s)u_0(q)\mathrm{d}\Omega(q) + \rho\int_\Omega u_0^*(q,t;s)v_0(q)\mathrm{d}\Omega(q)\Bigg\} + \int_0^t\int_\Omega u^*(Q,t;s,\tau)f(\tau)\mathrm{d}\tau
\end{aligned} \tag{9}$$

where Ω and Γ are, respectively, the domain and boundary of the problem. When the Green's function is null on Γ_u (where essential conditions are prescribed), which is the case of $\mathbf{G}$ indicated in Eq. (6), the first integral on the r.h.s of Eq. (9) is restricted to Γ_p (where natural boundary conditions are prescribed, see [23]).

Note that BEM and ExGAH(or ExGA) compute initial conditions and boundary flux/load contributions in quite a similar way; however, boundary pressure/displacement contributions are computed differently for each method: in the ExGA pressure/displacement contribution is computed in a FEM way; the corresponding boundary integral indicated in expression (9) is not present in expression (6).

It is important to observe that Eq. (6) is quite general, i.e., it can be applied to any kind of physical model, e.g., anisotropic viscoelastic media, etc.; it is only necessary to establish a suitable methodology to compute the Green's function of the problem.

To calculate the numerical solution at $t + \Delta t$, as indicated by Eq. (8), the convolution integrals shown there must be computed numerically. Three alternatives to compute these convolution integrals are indicated below:

$$\int_t^{t+\Delta t} \mathbf{G}(t+\Delta t-\tau)\mathbf{F}(\tau)\mathrm{d}\tau = \int_0^{\Delta t} \mathbf{G}(\Delta t-\tau)\mathbf{F}(t+\tau)\mathrm{d}\tau \approx \left\{\sum_{j=1}^{k}\boldsymbol{\psi}_1(j)\right\}\mathbf{F}^t + \left\{\sum_{j=1}^{k}\boldsymbol{\psi}_2(j)\right\}\mathbf{F}^{t+\Delta t} \tag{10}$$

$$\int_0^{\Delta t} \mathbf{G}(\Delta t-\tau)\mathbf{F}(t+\tau)\mathrm{d}\tau \approx \left\{\sum_{j=1}^{k}\frac{1}{2}\boldsymbol{\psi}_1(j) + \frac{1}{2}\boldsymbol{\psi}_1(j-1)\right\}\mathbf{F}^t + \left\{\sum_{j=1}^{k}\frac{1}{2}\boldsymbol{\psi}_2(j) + \frac{1}{2}\boldsymbol{\psi}_2(j-1)\right\}\mathbf{F}^{t+\Delta t} \tag{11}$$

$$\begin{aligned}
\int_0^{\Delta t} \mathbf{G}(\Delta t-\tau)\mathbf{F}(t+\tau)\mathrm{d}\tau \approx &\left\{\sum_{j=1}^{k/2}\frac{1}{3}\boldsymbol{\psi}_1(2j) + \frac{4}{3}\boldsymbol{\psi}_1(2j-1) + \frac{1}{3}\boldsymbol{\psi}_1(2j-2)\right\}\mathbf{F}^t \\
&+ \left\{\sum_{j=1}^{k/2}\frac{1}{3}\boldsymbol{\psi}_2(2j) + \frac{4}{3}\boldsymbol{\psi}_2(2j-1) + \frac{1}{3}\boldsymbol{\psi}_2(2j-2)\right\}\mathbf{F}^{t+\Delta t}
\end{aligned} \tag{12}$$

where $\boldsymbol{\psi}_1(j) = \left(1-\frac{j}{k}\right)\frac{\Delta t}{k}\mathbf{G}\left(\Delta t - \frac{j\Delta t}{k}\right)$ and $\boldsymbol{\psi}_2(j) = \frac{j}{k}\frac{\Delta t}{k}\mathbf{G}\left(\Delta t - \frac{j\Delta t}{k}\right)$.

Eq. (10) is very simple (Rectangle rule) and assumes that the integrand is constant for every sub-interval inside the range $[t, t + \Delta t]$. Approximation (11) is given by the Newton–Cotes formula where an interpolation polynomial of order 1 (Trapezoidal Rule) is generated for each equal sub-interval between $[t, t + \Delta t]$. Eq. (12) indicates that the integrand is approximated by a polynomial of order 2 (Simpson's 1/3 rule), thus the method needs three points; consequently the integer number k must be multiple of two. The convolution integral concerning the velocity vector is calculated by replacing the Green's matrix by its time derivative in the above equations.

The integer number k may be the sub-steps number n or a number less than n where values of $\mathbf{G}(t)$ are known. For example, when $n = 4$, the integer k has the following possibilities $k = 1, 2, 4$; when $n = 6$, the integer k may be $k = 1, 2, 3, 6$ and so on. However, the present method allows large Δt when sub-steps are employed, in which case linear time interpolation for $\mathbf{F}(t)$, as considered in Eqs. (10)–(12), may not be acceptable. In order to improve the linear approximation one may apply an h or p time refinement.

The Green's matrices at time $t = \Delta t$ must be calculated before using Eq. (8). Usually, texts of mathematic–physics (see [23,45]) present analytical expressions for Green's functions for homogeneous infinite domains; in elastic, acoustic or other similar wave propagation problem, the Green's function represents the response at a field point x, at time t, due to an impulsive signal applied at a source point s, at time $t = \tau$. Here, Green's functions are obtained via numerical methods (FDM in present paper), thus they can refer to any physical medium. Furthermore, the Green's function can be made to obey the problem boundary conditions, or any other that may be adequate; however, employing a numerical method to compute Green's functions may be too expensive. It is important to notice that this is not the case here as the complete Green's function time history is not required: only values of $\mathbf{G}(t)$ at $t = \Delta t$ or at sub-steps are necessary, as a step-by-step time marching scheme is employed to integrate the governing equations (see expression (8)). The physical relation "impulse equals momentum variation" permits computation of the problem Green's function $g_j(\mathbf{x}_i, t)$, corresponding to an impulsive source located at point j of the grid applied at time $\tau = 0$, by solving Eq. (13) (K has been admitted homogenous), considering the following initial conditions: $g_j(x_i, 0) = 0$; $\dot{g}_j(x_i, 0) = \delta_{ij}/\rho$ (see [25,28,29]):

$$K\nabla^2 g_j(\mathbf{x}, t) - c\dot{g}_j(\mathbf{x}, t) - \rho\ddot{g}_j(\mathbf{x}, t) = 0 \tag{13}$$

As mentioned before, Eq. (13) is spatially discretized by the FDM in the present work: a second or fourth-order finite difference discrete operator was used as an approximation to the spatial derivatives indicated. The final algebraic equations written in matrix form read

$$\begin{aligned} &\mathbf{M}\ddot{\mathbf{G}}(t) + \mathbf{C}\dot{\mathbf{G}}(t) + \mathbf{K}\mathbf{G}(t) = \mathbf{0} \\ &\mathbf{G}(0) = \mathbf{0} \\ &\dot{\mathbf{G}}(0) = \mathbf{M}^{-1} \end{aligned} \tag{14}$$

where $\mathbf{G}(t)$, $\dot{\mathbf{G}}(t)$ and $\ddot{\mathbf{G}}(t)$ are the Green's matrices of the problem. Note that each column j of the Green's matrix represents the Green's function $g_j(\mathbf{x}_i, t)$ of the problem governed by Eq. (13), subjected to homogeneous boundary conditions. Eq. (14) is a more convenient notation to represent the calculation of the entries of the Green's matrices. Finding the solution of Eq. (14) seems to be expensive; however, it may become cheap if one observes that when finding a column, say j, of matrix $\mathbf{G}(t)$, one is in fact computing the Green's function for a source applied at node j. Thus only a sub-domain, or rather a sub-mesh, in the neighborhood of node j must be considered. It is important to observe that the adopted sub-domain region may be a little larger than the one estimated theoretically, in order to minimize errors, especially when a large number of sub-steps is considered.

It is important to notice that mass matrices are lumped in the finite difference scheme employed here to compute the Green's matrices required by the ExGA method. Lumped matrices lead to explicit algorithms, which drastically decrease computational efforts. However, in many cases, explicit algorithms lead to less accurate and conditionally stable analysis. The use of sub-steps, as illustrated here, makes the ExGA algorithm more accurate and unconditionally stable for practical purposes, since critical time step values can be made as large as one wishes, by increasing the number of sub-steps.

4. The ExGA-Runge–Kutta method (ExGA-RK)

A time-marching algorithm is used to find numerical solutions of Eq. (14). In this work the Runge–Kutta and the central difference schemes are considered. It can be shown that the explicit form of the classical fourth-order Runge–Kutta method for hyperbolic problems can be written as

$$\begin{aligned}
\mathbf{W}_1 &= \mathbf{M}^{-1}(-\mathbf{K}\mathbf{G}^t - \mathbf{C}\dot{\mathbf{G}}^t)\\
\mathbf{W}_2 &= \mathbf{M}^{-1}\left(-\mathbf{K}\left(\mathbf{G}^t + \frac{1}{2}\frac{\Delta t}{n}\dot{\mathbf{G}}^t\right) - \mathbf{C}\left(\dot{\mathbf{G}}^t + \frac{1}{2}\frac{\Delta t}{n}\mathbf{W}_1\right)\right)\\
\mathbf{W}_3 &= \mathbf{M}^{-1}\left(-\mathbf{K}\left(\mathbf{G}^t + \frac{1}{2}\frac{\Delta t}{n}\dot{\mathbf{G}}^t + \frac{1}{4}\frac{\Delta t^2}{n^2}\mathbf{W}_1\right) - \mathbf{C}\left(\dot{\mathbf{G}}^t + \frac{1}{2}\frac{\Delta t}{n}\mathbf{W}_2\right)\right)\\
\mathbf{W}_4 &= \mathbf{M}^{-1}\left(-\mathbf{K}\left(\mathbf{G}^t + \frac{\Delta t}{n}\dot{\mathbf{G}}^t + \frac{1}{2}\frac{\Delta t^2}{n^2}\mathbf{W}_2\right) - \mathbf{C}\left(\dot{\mathbf{G}}^t + \frac{\Delta t}{n}\mathbf{W}_3\right)\right)
\end{aligned} \tag{15}$$

The displacement and velocity Green matrices are evaluated by

$$\begin{aligned}
\mathbf{G}^{t+\frac{\Delta t}{n}} &= \mathbf{G}^t + \frac{\Delta t}{n}\dot{\mathbf{G}}^t + \frac{1}{6}\frac{\Delta t^2}{n^2}(\mathbf{W}_1 + \mathbf{W}_2 + \mathbf{W}_3)\\
\dot{\mathbf{G}}^{t+\frac{\Delta t}{n}} &= \dot{\mathbf{G}}^t + \frac{1}{6}\frac{\Delta t}{n}(\mathbf{W}_1 + 2\mathbf{W}_2 + 2\mathbf{W}_3 + \mathbf{W}_4)
\end{aligned} \tag{16}$$

Expression (16) is general and the ExGA-RK approach requires the computation of $\mathbf{G}^{\Delta t}$ and $\dot{\mathbf{G}}^{\Delta t}$. The Green's matrices $\mathbf{G}^{\Delta t}$ and $\dot{\mathbf{G}}^{\Delta t}$ can be obtained in one step by making $n = 1$ in expressions (15) and (16), or by employing n sub-steps within the time step Δt. When sub-stepping is employed, stability conditions and accuracy are substantially improved. If an adequate number of sub-steps is employed, the critical time step can become so large that, for all practical purposes, explicit Green's function based time stepping algorithms become unconditionally stable. Accuracy is also drastically improved, so that, having a good time history picture will be the factor defining the time step length.

5. Stability of the ExGA-RK and Runge–Kutta methods

To examine the stability properties of direct integration methods, the dynamic equilibrium equation of a single-degree-of-freedom mechanical system can be used (see Eq. (3)). The conclusions apply to multi-degree-of-freedom systems as well, because when a modal basis is employed, the uncoupled equations are similar to Eq. (3). When a SDOF is considered, Eq. (8) can be represented by the following recursive expression:

$$\begin{bmatrix} u^{t+\Delta t} \\ \dot{u}^{t+\Delta t} \end{bmatrix} = \begin{bmatrix} \dot{g}(\Delta t) + 2\xi\omega g(\Delta t) & g(\Delta t) \\ \ddot{g}(\Delta t) + 2\xi\omega\dot{g}(\Delta t) & \dot{g}(\Delta t) \end{bmatrix} \begin{bmatrix} u^t \\ \dot{u}^t \end{bmatrix} + \begin{bmatrix} L_{11} & L_{12} \\ L_{21} & L_{22} \end{bmatrix} \begin{bmatrix} f^t \\ f^{t+\Delta t} \end{bmatrix} = \mathbf{A}\begin{bmatrix} u^t \\ \dot{u}^t \end{bmatrix} + \mathbf{L}\begin{bmatrix} f^t \\ f^{t+\Delta t} \end{bmatrix} \tag{17}$$

where $\mathbf{A}$ represents the amplification matrix and the load operator is represented by matrix $\mathbf{L}$. Note that the load operator is obtained here for external loads that vary linearly within $[t, t + \Delta t]$, as presented by expressions (10)–(12).

The stability condition requires that matrix $\mathbf{A}$ does not amplify errors as the time-step algorithm advances on time. The condition required to assure stability is [32,33]:

$$\rho(\mathbf{A}) \leqslant 1 \tag{18}$$

where $\rho(\mathbf{A})$ is the spectral radius of matrix $\mathbf{A}$, $\rho(\mathbf{A}) = \max|\lambda_i|$, where the eigenvalues λ_i are obtained from the solution of the eigenvalue problem $\mathbf{A}\mathbf{v} = \lambda\mathbf{v}$.

Taking into account expressions (15) and (16) for the Runge–Kutta method, the numerical Green's functions $g(\Delta t)$ and $\dot{g}(\Delta t)$ are given by the following recursive matrix relation:

$$\begin{bmatrix} g(\Delta t) \\ \dot{g}(\Delta t) \end{bmatrix} = \begin{bmatrix} A_{11}\left(\frac{\Delta t}{n}\right) & A_{12}\left(\frac{\Delta t}{n}\right) \\ A_{21}\left(\frac{\Delta t}{n}\right) & A_{22}\left(\frac{\Delta t}{n}\right) \end{bmatrix}^n \begin{bmatrix} g(0) \\ \dot{g}(0) \end{bmatrix} \tag{19}$$

where $g(0) = 0$, $\dot{g}(0) = 1$ and

$$A_{11}\left(\frac{\Delta t}{n}\right) = \frac{1}{24}\left(24 - 12\frac{\Delta t^2}{n^2}\omega^2 + 8\frac{\Delta t^3}{n^3}\omega^3\xi + (1-4\xi^2)\frac{\Delta t^4}{n^4}\omega^4\right)$$
$$A_{12}\left(\frac{\Delta t}{n}\right) = \frac{-1}{6}\frac{\Delta t}{n}\left(-6 + 6\xi\frac{\Delta t}{n}\omega + (1-4\xi^2)\frac{\Delta t^2}{n^2}\omega^2 + \xi(-1+2\xi^2)\frac{\Delta t^3}{n^3}\omega^3\right)$$
$$A_{21}\left(\frac{\Delta t}{n}\right) = \frac{1}{6}\frac{\Delta t}{n}\omega^2\left(-6 + 6\xi\frac{\Delta t}{n}\omega + (1-4\xi^2)\frac{\Delta t^2}{n^2}\omega^2 + \xi(-1+2\xi^2)\frac{\Delta t^3}{n^3}\omega^3\right)$$
$$A_{22}\left(\frac{\Delta t}{n}\right) = \frac{1}{24}\left(24 - 48\xi\frac{\Delta t}{n}\omega + 16\xi(1-2\xi^2)\frac{\Delta t^3}{n^3}\omega^3 + 12(-1+4\xi^2)\frac{\Delta t^2}{n^2}\omega^2 + (1-12\xi^2+16\xi^4)\frac{\Delta t^4}{n^4}\omega^4\right) \tag{20}$$

Applying Eqs. (19) and (20) into the amplification matrix **A** shown in Eq. (17), having in mind that $\ddot{g}(\Delta t)$ is calculated from the equilibrium equation, i.e., $\ddot{g}(\Delta t) = -2\xi\omega\dot{g}(\Delta t) - \omega^2 g(\Delta t)$, it becomes possible to solve the eigenvalue problem and to compute the amplification spectral matrix radius. The expression for the spectral radius, when $\xi = 0$, is given below, as a function of the number of sub-steps n and of $\Delta t/T$, where $T = 2\pi/\omega$ is the natural period:

$$\rho(\mathbf{A}, n) = 3^{-n}\left(a - 2\frac{b}{\sqrt{-n^6}}\right)^{\frac{n}{2}}\left(a + 2\frac{b}{\sqrt{-n^6}}\right)^{\frac{n}{2}} \tag{21}$$

where

$$a = 3 - \frac{6\pi^2}{n^2}\frac{\Delta t^2}{T^2} + \frac{2\pi^4}{n^4}\frac{\Delta t^4}{T^4}$$
$$b = 3n^2\pi\frac{\Delta t}{T} - 2\pi^3\frac{\Delta t^3}{T^3}$$

Fig. 1 shows that stability conditions can be relaxed when sub-steps are considered. When $n = 1$ the present method has the same stability restrictions as the Runge–Kutta scheme, both of them are stable as long as $\Delta t/T$ is less than $\sqrt{2}/\pi$. For $n = 2$ the present method stability condition is given by $\Delta t/T \leqslant 2\sqrt{2}/\pi$. It can be demonstrated that the critical value of $\Delta t/T$ varies linearly with n, i.e., the stability condition is: $\Delta t/T \leqslant n\sqrt{2}/\pi$.

6. Truncation errors of the load operator for the ExGA-RK method

In order to measure the error caused by the numerical integration of the convolution integrals, the analytical load operator $\mathbf{L}_{AN}$ can be compared with the numerical one. Assuming that the force is linear between the time step $[0, \Delta t]$, the convolution integrals, for $\xi = 0$, can be written as (see Eq. (5)):

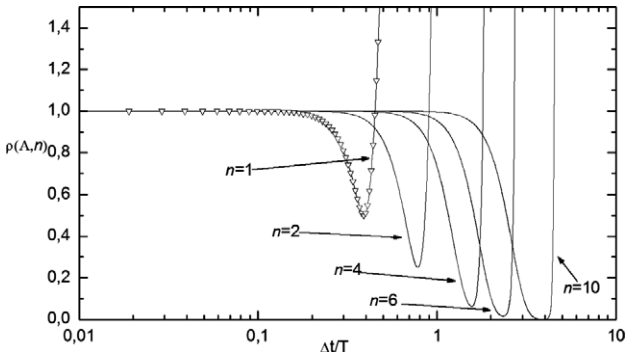

Fig. 1. Spectral radius related to the (—) ExGA-RK and (▽) Runge–Kutta schemes for the undamped case ($\xi = 0.0$).

$$\int_0^{\Delta t} g(\Delta t-\tau)f(\tau)\mathrm{d}\tau = \int_0^{\Delta t} \frac{1}{\omega}\sin(\omega(\Delta t-\tau))\left[\left(\frac{f(\Delta t)-f(0)}{\Delta t}\right)\tau + f(0)\right]\mathrm{d}\tau$$
$$\int_0^{\Delta t} \dot{g}(\Delta t-\tau)f(\tau)\mathrm{d}\tau = \int_0^{\Delta t} \cos(\omega(\Delta t-\tau))\left[\left(\frac{f(\Delta t)-f(0)}{\Delta t}\right)\tau + f(0)\right]\mathrm{d}\tau \tag{22}$$

After Eq. (22) is integrated, it can be put in a matrix form as indicated below:

$$\mathbf{L}_{\mathrm{AN}} = \begin{bmatrix} \frac{\cos(\omega\Delta t)}{\omega^2}+\frac{\sin(\omega\Delta t)}{\omega^3\Delta t} & \frac{1}{\omega^2}-\frac{\sin(\omega\Delta t)}{\omega^3\Delta t} \\ -\frac{1}{\omega^2\Delta t}+\frac{\cos(\omega\Delta t)}{\omega^2\Delta t}+\frac{\sin(\omega\Delta t)}{\omega} & \frac{1}{\omega^2\Delta t}-\frac{\cos(\omega\Delta t)}{\omega^2\Delta t} \end{bmatrix} \tag{23}$$

which can be expanded in Taylor's series as follows:

$$\begin{aligned} L_{\mathrm{AN}}(1,1) &= \frac{\Delta t^2}{3}-\frac{\omega^2\Delta t^4}{30}+\frac{\omega^4\Delta t^6}{840}-\frac{\omega^6\Delta t^8}{45360}+\frac{\omega^8\Delta t^{10}}{3991680}-\cdots \\ L_{\mathrm{AN}}(1,2) &= \frac{\Delta t^2}{6}-\frac{\omega^2\Delta t^4}{120}+\frac{\omega^4\Delta t^6}{5040}-\frac{\omega^6\Delta t^8}{362880}+\frac{\omega^8\Delta t^{10}}{39916800}-\cdots \\ L_{\mathrm{AN}}(2,1) &= \frac{\Delta t}{2}-\frac{\omega^2\Delta t^3}{8}+\frac{\omega^4\Delta t^5}{144}-\frac{\omega^6\Delta t^7}{5760}+\frac{\omega^8\Delta t^9}{403200}-\cdots \\ L_{\mathrm{AN}}(2,2) &= \frac{\Delta t}{2}-\frac{\omega^2\Delta t^3}{24}+\frac{\omega^4\Delta t^5}{720}-\frac{\omega^6\Delta t^7}{40320}+\frac{\omega^8\Delta t^9}{3628800}-\cdots \end{aligned} \tag{24}$$

The numerical load operator matrix obtained using Eq. (10) is indicated by Eq. (25) below:

$$\mathbf{L}_1 = \begin{bmatrix} \sum_{j=1}^{k}\frac{k-j}{k^2}\Delta t g\left(\Delta t-\frac{j}{k}\Delta t\right) & \sum_{j=1}^{k}\frac{j}{k^2}\Delta t g\left(\Delta t-\frac{j}{k}\Delta t\right) \\ \sum_{j=1}^{k}\frac{k-j}{k^2}\Delta t \dot{g}\left(\Delta t-\frac{j}{k}\Delta t\right) & \sum_{j=1}^{k}\frac{j}{k^2}\Delta t \dot{g}\left(\Delta t-\frac{j}{k}\Delta t\right) \end{bmatrix} \tag{25}$$

The load operator matrix indicated by expression (25) is denoted $\mathbf{L}_1$. Eqs. (11) and (12) can be used to generate load operator matrices denoted here, respectively, by $\mathbf{L}_2$ and $\mathbf{L}_3$. It is important to observe that discrete values of $g(\tau)$ are required in order to numerically compute the convolution integrals previously indicated. Thus, it is appropriate to adopt $k=n$, i.e., all the values of $g(\tau)$, obtained through sub-stepping, are used to evaluate expressions (10), (11) or (12). Having in mind that the Runge–Kutta scheme is being adopted to calculate the Green's function terms, the load operator entries may be obtained, as presented in Table 1, for $\mathbf{L}_1$, $\mathbf{L}_2$ and $\mathbf{L}_3$, and $n=1$ and $n=2$.

A comparison of expressions (24) with Table 1 shows that the errors of the load operator entries decrease as n increases. As expected, the load operator matrix $\mathbf{L}_3$ produces better results than the others. As shown in the

Table 1
Entries of the load operator matrix for the ExGA-RK method

	$n=k=1$	$n=k=2$
$\mathbf{L}_1$	$L_1(1,1)=0$	$L_1(1,1)=L_1(1,2)=\frac{\Delta t^2}{8}-\frac{\omega^2\Delta t^4}{192}$
	$L_1(1,2)=0$	$L_1(2,1)=\frac{\Delta t}{4}-\frac{\omega^2\Delta t^3}{32}+\frac{\omega^4\Delta t^5}{1536}$
	$L_1(2,1)=0$	$L_1(2,2)=\frac{3\Delta t}{4}-\frac{\omega^2\Delta t^3}{32}+\frac{\omega^4\Delta t^5}{1536}$
	$L_1(2,2)=\Delta t$	
$\mathbf{L}_2$	$L_2(1,1)=\frac{\Delta t^2}{2}-\frac{\omega^2\Delta t^4}{12}$	$L_2(1,1)=\frac{3\Delta t^2}{2}-\frac{3\omega^2\Delta t^4}{64}+\frac{\omega^4\Delta t^6}{512}-\frac{\omega^6\Delta t^8}{36864}$
	$L_2(1,2)=0$	$L_2(1,2)=\frac{\Delta t^2}{8}-\frac{\omega^2\Delta t^4}{192}$
	$L_2(2,1)=\frac{\Delta t}{2}-\frac{\omega^2\Delta t^3}{4}+\frac{\omega^4\Delta t^5}{48}$	$L_2(2,1)=\frac{\Delta t}{2}-\frac{5\omega^2\Delta t^3}{32}+\frac{17\omega^4\Delta t^5}{1536}-\frac{5\omega^6\Delta t^7}{18432}+\frac{\omega^8\Delta t^9}{589824}$
	$L_2(2,2)=\frac{\Delta t}{2}$	$L_2(2,2)=\frac{\Delta t}{2}-\frac{\omega^2\Delta t^3}{32}+\frac{\omega^4\Delta t^5}{1536}$
$\mathbf{L}_3$	–	$L_3(1,1)=\frac{\Delta t^2}{3}-\frac{5\omega^2\Delta t^4}{144}+\frac{\omega^4\Delta t^6}{768}-\frac{\omega^6\Delta t^8}{55296}$
		$L_3(1,2)=\frac{\Delta t^2}{6}-\frac{\omega^2\Delta t^4}{144}$
		$L_3(2,1)=\frac{\Delta t}{2}-\frac{\omega^2\Delta t^3}{8}+\frac{\omega^4\Delta t^5}{128}-\frac{5\omega^6\Delta t^7}{27648}+\frac{\omega^8\Delta t^9}{884736}$
		$L_3(2,2)=\frac{\Delta t}{2}-\frac{\omega^2\Delta t^3}{24}+\frac{\omega^4\Delta t^5}{1152}$

following sections, the errors introduced by the amplification matrix **A** are higher than those caused by the load operator **L**.

One should not be misled by the powers of ω in Table 1 (and, as a consequence, an erroneous interpretation of several stiffness matrix multiplications in a MDOF system), which appears due to the Taylor's series expansion. The evaluation of the load convolution integral for MDOF systems is not expensive if one notices that the force is interpolated within the time interval. Thus, computation of **L** factors is required only at the first time step. Numerical Green's matrices are employed to compute $\boldsymbol{\psi}_1$ and $\boldsymbol{\psi}_2$ (see expressions (10)–(12)), which are stored and used for all subsequent time steps: only simple products by the vector force entries by corresponding coefficients are then required.

7. Accuracy of the ExGA-RK and the Runge–Kutta methods

The influence of the numerical dissipation and numerical dispersion have to be considered for a complete analysis of performance. These two characteristics can be, respectively, measured by the expression of the algorithm damping ratio $\bar{\xi}$ and relative period error $(\overline{T}-T)/T$, where $T=2\pi/\omega$ and $\overline{T}=2\pi/\bar{\omega}$. Numerical errors can also be estimated solving an initial value problem where the relative period error and the amplitude decay AD are calculated numerically (see [33]). Alternatively, the analytical expression for algorithm damping ratio and relative period error can be defined in terms of the principal roots $\lambda_{1,2}$ of the eigenvalue problem as shown below (see [3,8,32,46]). Thus, the amplitude decay AD can be approximated by the following form $AD \approx 2\pi\bar{\xi}$ and the relative period error is given by $(\overline{T}-T)/T=(\omega-\bar{\omega})/\bar{\omega}$ (see [32]):

$$\begin{aligned}\bar{\omega} &= \frac{\arctan(B/A)}{\Delta t\sqrt{1-\xi^2}} \\ \bar{\xi} &= \frac{-\ln(A^2+B^2)\sqrt{1-\xi^2}}{2\arctan(B/A)}\end{aligned} \tag{26}$$

Parameters A and B of the expressions shown above are obtained from the following equation:

$$\lambda_{1,2} = A \pm Bi = \sqrt{A^2+B^2}\exp\left(\pm\arctan\left(\frac{B}{A}\right)i\right) = \exp\left(-\bar{\xi}\bar{\omega}\Delta t \pm \bar{\omega}\sqrt{1-\xi^2}\Delta t i\right) \tag{27}$$

Fig. 2a and b shows, respectively, that the algorithm damping ratio and relative period error decrease when sub-stepping is used. When $n=1$ the ExGA-Runge–Kutta method has the same accuracy as the original Runge–Kutta. Low values of n are sufficient to enhance considerably the range of permitted time-step values.

8. The ExGA-Central Difference method (ExGA-CD)

When central differences in time are used to calculate the Green's matrix, the following recursive expression is obtained:

$$\mathbf{G}^{t+\frac{\Delta t}{n}} = \left(\frac{n^2}{\Delta t^2}\mathbf{M}+\frac{n}{2\Delta t}\mathbf{C}\right)^{-1}\left(\left(\frac{2n^2}{\Delta t^2}\mathbf{M}-\mathbf{K}\right)\mathbf{G}^{t}+\left(-\frac{n^2}{\Delta t^2}\mathbf{M}+\frac{n}{2\Delta t}\mathbf{C}\right)\mathbf{G}^{t-\frac{\Delta t}{n}}\right) \tag{28}$$

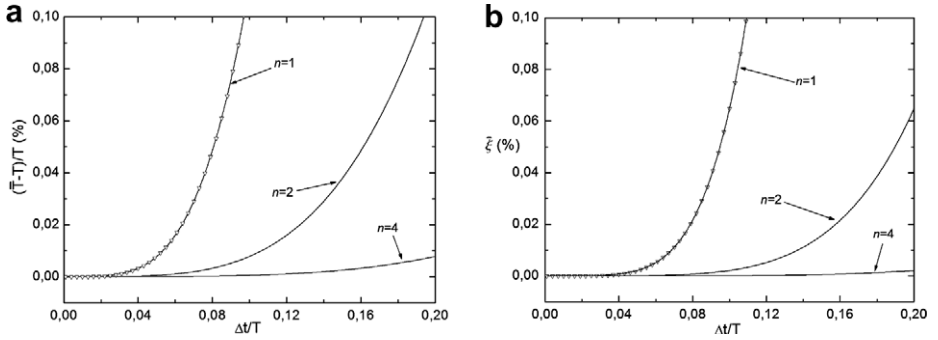

Fig. 2. Accuracy of the (—) ExGA-RK and (▽) Runge–Kutta schemes: (a) relative period error and (b) numerical damping ratio.

where

$$\mathbf{G}^{-\frac{\Delta t}{n}} = \mathbf{G}^0 - \frac{\Delta t}{n}\dot{\mathbf{G}}^0 + \frac{\Delta t^2}{2n^2}\ddot{\mathbf{G}}^0$$
$$\ddot{\mathbf{G}}^0 = \mathbf{M}^{-1}(-\mathbf{C}\dot{\mathbf{G}}^0 - \mathbf{K}\mathbf{G}^0)$$

The spectral radius of the amplification matrix shown in expression (17) must be computed in order to analyze the stability condition of the ExGA-Central Difference method. The Green's function is evaluated through expression (29) below:

$$\begin{bmatrix} g(\Delta t) \\ g(0) \end{bmatrix} = \begin{bmatrix} \dfrac{2-\omega^2\Delta t^2/n^2}{1+\xi\omega\Delta t/n} & \dfrac{-1+\xi\omega\Delta t/n}{1+\xi\omega\Delta t/n} \\ 1 & 0 \end{bmatrix}^n \begin{bmatrix} g(0) \\ g\left(-\frac{\Delta t}{n}\right) \end{bmatrix} \tag{29}$$

where $g(0) = 0$, $\dot{g}(0) = 1$, $\ddot{g}(0) = -2\xi\omega\dot{g}(0) - \omega^2 g(0)$ and $g\left(-\frac{\Delta t}{n}\right) = g(0) - \frac{\Delta t}{n}\dot{g}(0) + \frac{\Delta t^2}{2n^2}\ddot{g}(0)$.

The Green's function first and second time derivatives can be calculated by

$$\begin{aligned} \dot{g}(\Delta t) &= \frac{n}{2\Delta t}\left(g\left(\Delta t + \frac{\Delta t}{n}\right) - g\left(\Delta t - \frac{\Delta t}{n}\right)\right) \\ \ddot{g}(\Delta t) &= \frac{n^2}{\Delta t^2}\left(g\left(\Delta t + \frac{\Delta t}{n}\right) - 2g(\Delta t) + g\left(\Delta t - \frac{\Delta t}{n}\right)\right) \end{aligned} \tag{30}$$

The amplification matrix for the ExGA-CD method is obtained by substituting $g(\Delta t)$, $\dot{g}(\Delta t)$ and $\ddot{g}(\Delta t)$, given by Eqs. (29) and (30), into Eq. (17). The spectral radius for the present case, when $\xi = 0$, can be computed by

$$\rho(\mathbf{A}, n) = \left(\frac{4^{-1-n}}{c}\left(4n^2\left(a - \frac{4}{n^2}\sqrt{b}\right)^n\left(a + \frac{4}{n^2}\sqrt{b}\right)^n + \frac{n^2}{4}(a-2)\left(\left(a - \frac{4}{n^2}\sqrt{b}\right)^n + \left(a + \frac{4}{n^2}\sqrt{b}\right)^n\right)^2\right)\right)^{1/2} \tag{31}$$

where

$$a = 2 - \frac{4\pi^2}{n^2}\frac{\Delta t^2}{T^2}$$
$$b = -n^2\pi^2\frac{\Delta t^2}{T^2} + \pi^4\frac{\Delta t^4}{T^4}$$
$$c = n^2 - \pi^2\frac{\Delta t^2}{T^2}$$

Fig. 3 depicts results for $\rho(\mathbf{A}, n)$ versus $\Delta t/T$, taking into account several values for n. The curve for the central difference method is constant, $\rho(\mathbf{A}) = 1$, until the stability limit is reached; at this point, $\rho(\mathbf{A}) \to \infty$. The $\rho(\mathbf{A}, n)$ versus $\Delta t/T$ curve for the ExGA-CD method, for $n = 1$, shows that $\lim_{\Delta t/T \to 0}\rho(\mathbf{A}, n) = 1$; in fact such an asymptotic behavior occurs for all values of n. For small values of $\Delta t/T$, the ExGA-CD method may have stability; however, the method breaks down much before the standard central difference approach. For values of n other than one, the $\rho(\mathbf{A}, n)$ versus $\Delta t/T$ curve displays an oscillatory behavior; it is possible to observe in Fig. 3 that the oscillation amplitude decreases as n increases, indicating that stability restrictions may be relaxed for some values of n. However, as shown in Fig. 5a and b, the accuracy of the ExGA-CD method is acceptable only for low values of $\Delta t/T$. A close analysis of Fig. 3 indicates that $\rho(\mathbf{A}, n) \geqslant 1$ for the ExGA-CD method, thus, it should be considered as unconditionally unstable.

9. The ExGAH-Central Difference method (ExGAH-CD)

As shown in the last section, the ExGA-Central Difference method is unconditionally unstable. Stability can be improved substantially if the contribution of $\mathbf{U}^t$ to $\mathbf{U}^{t+\Delta t}$ is computed by superposition in space of the contributions of individual nodes transferred in time by the step response function. In this case the

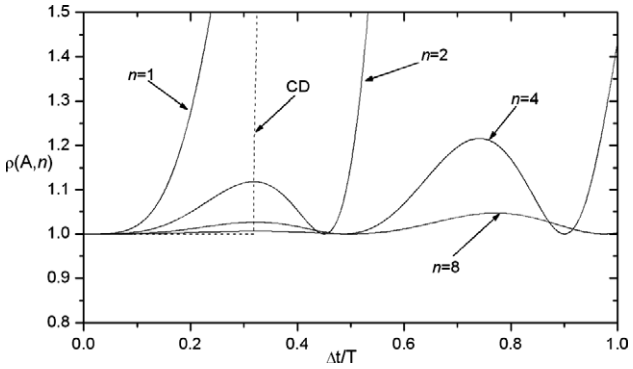

Fig. 3. Spectral radius related to the (—) ExGA-CD and (----) Central Difference schemes for the undamped case ($\xi = 0.0$).

transference of the $\mathbf{U}^t$ contribution to $\mathbf{U}^{t+\Delta t}$ is carried out by the product of $\mathbf{H}(\Delta t)\mathbf{M}\mathbf{U}^t$, as discussed next. The transfer step response matrix $\mathbf{H}(\Delta t)$ has been used previously, in a context similar to that of the present work, in [30,31,13]. Thus, for the SDOF case, the ExGAH integral equation reads

$$u(t) = h(t)u(0) + g(t)\dot{u}(0) + \int_0^t g(t-\tau)f(\tau)\mathrm{d}\tau \tag{32}$$

Comparison of Eqs. (32) and (4) shows that:

$$\begin{aligned} h(t) &= \dot{g}(t) + 2\xi\omega g(t) \\ \dot{h}(t) &= \ddot{g}(t) + 2\xi\omega\dot{g}(t) \end{aligned} \tag{33}$$

Eq. (32) shows that $h(t)$ is the time response of the SDOF mechanical system, due to the following initial conditions: $h(0) = 1$ and $\dot{h}(0) = 0$. Thus, instead of employing the r.h.s of Eq. (33), with $\dot{g}(t)$ obtained from the solution of Eq. (13), to transfer $u(0)$ contribution to $u(t)$, substantial stability conditions improvements are obtained if $h(t)$ is computed independently.

Expressions (32) and (33) can also be employed in nodal analyses; when physical coordinates are used for MDOF systems, the following matrix expressions for $\mathbf{U}$ and $\dot{\mathbf{U}}$ arise:

$$\mathbf{U}^{t+\Delta t} = \mathbf{H}(\Delta t)\mathbf{M}\mathbf{U}^t + \mathbf{G}(\Delta t)\mathbf{M}\dot{\mathbf{U}}^t + \int_t^{t+\Delta t} \mathbf{G}(t+\Delta t-\tau)\mathbf{F}(\tau)\mathrm{d}\tau \tag{34}$$

$$\dot{\mathbf{U}}^{t+\Delta t} = \dot{\mathbf{H}}(\Delta t)\mathbf{M}\mathbf{U}^t + \dot{\mathbf{G}}(\Delta t)\mathbf{M}\dot{\mathbf{U}}^t + \int_t^{t+\Delta t} \dot{\mathbf{G}}(t+\Delta t-\tau)\mathbf{F}(\tau)\mathrm{d}\tau \tag{35}$$

Eqs. (34) and (35) require the calculation of the step response matrix $\mathbf{H}(\Delta t)$ and of the Green's matrix $\mathbf{G}(\Delta t)$, as well as their time derivatives. The calculation of the Green's matrix was presented in previous sections and the discussion presented next is concerned with obtaining $\mathbf{H}(\Delta t)$ and $\dot{\mathbf{H}}(\Delta t)$. Expression (34) shows, as commented previously, that the step response matrix transfers $\mathbf{U}^0$ to $\mathbf{U}^{\Delta t}$ (or $\mathbf{U}^t$ to $\mathbf{U}^{t+\Delta t}$) through superposition of responses of initial conditions at each node given by the product of the node shape function times the value of the initial displacement at that node. Thus, $\mathbf{H}$ and $\dot{\mathbf{H}}$ are obtained by a procedure similar to that employed to compute $\mathbf{G}$ and $\dot{\mathbf{G}}$, i.e., from the solution of the homogeneous version of Eq. (1). However, differently from the Green's function, the step response function is calculated with non-null initial displacement and null initial velocity, as indicated next:

$$\begin{aligned} &\mathbf{M}\ddot{\mathbf{H}}(t) + \mathbf{C}\dot{\mathbf{H}}(t) + \mathbf{K}\mathbf{H}(t) = \mathbf{0} \\ &\mathbf{H}^0 = \mathbf{M}^{-1} \\ &\dot{\mathbf{H}}^0 = 0 \end{aligned} \tag{36}$$

The amplification matrix for the ExGAH-CD method, for a SDOF mechanical system, can be expressed as indicated by Eq. (37):

$$\mathbf{A} = \begin{bmatrix} h(\Delta t) & g(\Delta t) \\ \dot{h}(\Delta t) & \dot{g}(\Delta t) \end{bmatrix} \tag{37}$$

The step response function can be calculated numerically, by the central difference scheme, as

$$\begin{bmatrix} h(\Delta t) \\ h(0) \end{bmatrix} = \begin{bmatrix} \dfrac{2-\omega^2\Delta t^2/n^2}{1+\xi\omega\Delta t/n} & \dfrac{-1+\xi\omega\Delta t/n}{1+\xi\omega\Delta t/n} \\ 1 & 0 \end{bmatrix}^n \begin{bmatrix} h(0) \\ h\left(-\frac{\Delta t}{n}\right) \end{bmatrix} \tag{38}$$

where $h(0) = 1$, $\dot{h}(0) = 0$, $\ddot{h}(0) = -2\xi\omega\dot{h}(0) - \omega^2 h(0)$ and $h\left(-\frac{\Delta t}{n}\right) = h(0) - \frac{\Delta t}{n}\dot{h}(0) + \frac{\Delta t^2}{2n^2}\ddot{h}(0)$

Fig. 4 depicts the variation of the spectral radius versus $\Delta t/T$, when sub-steps are considered. As can be seen, the ExGAH – CD algorithm provides a conditionally stable scheme were the critical value of $\Delta t/T$ increases as n increases. For $n = 1$ the present method has the same stability characteristics as the traditional central difference method as well as equivalent accuracy, as shown by the graphics on Figs. 4 and 5a,b. For $n = 2$, the ExGAH-CD method becomes unstable when $\Delta t/T$ is greater than $2/\pi$. The analyses carried out by the present work show that the critical value for $\Delta t/T$ has linear variation with n, expressed by $\Delta t/T \leqslant n/\pi$. This is an important result as it renders unnecessary to develop approximate expressions to estimate $\rho(\mathbf{A}, n)$, having in mind that the value of the spectral radius is equal to one until it reaches its critical value. Furthermore, the method accuracy improves substantially with just a few sub-steps n, as can be seen in Fig. 5a and b.

10. Truncation errors of the amplification matrix

From the Lax equivalence theorem, the scheme is said to be convergent if it is stable and consistent. The stability has already been discussed above and the consistency is studied by analyzing the truncation error of

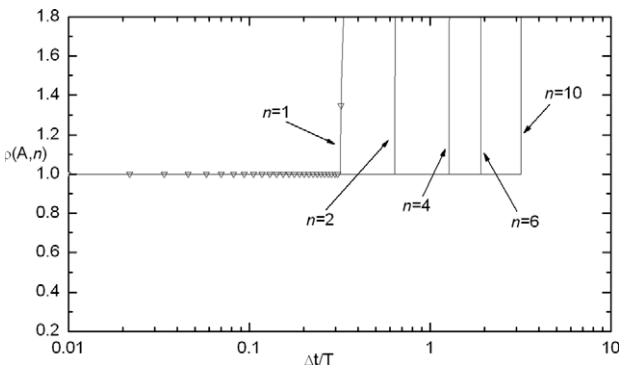

Fig. 4. Spectral radius related to the (—) ExGAH-CD and (▽) Central Difference schemes for the undamped case ($\xi = 0.0$).

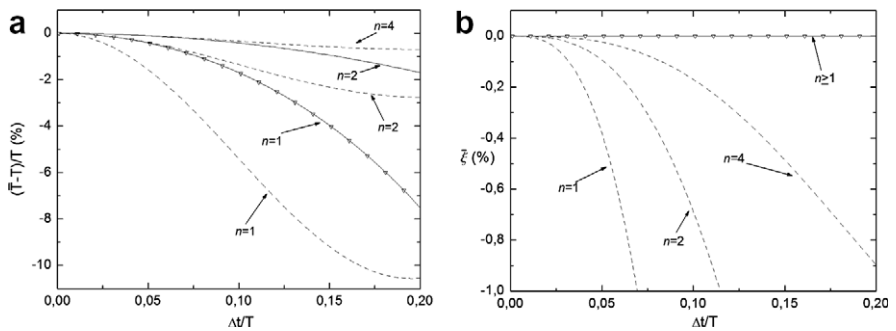

Fig. 5. Accuracy of the (-----) ExGA-CD, (—-) ExGAH-CD and (▽) Central Difference schemes: (a) relative period error and (b) numerical damping ratio.

the numerical amplification matrix when it is compared with the analytical one. The analytical amplification matrix for a SDOF is given by (see [34,37,42]):

$$\mathbf{A}_{\mathrm{AN}} = \mathrm{e}^{-\xi\omega\Delta t}\begin{pmatrix} \cos(\omega_{\mathrm{d}}\Delta t) + \frac{\xi\omega}{\omega_{\mathrm{d}}}\sin(\omega_{\mathrm{d}}\Delta t) & \frac{1}{\omega_{\mathrm{d}}}\sin(\omega_{\mathrm{d}}\Delta t) \\ -\frac{\omega^2}{\omega_{\mathrm{d}}}\sin(\omega_{\mathrm{d}}\Delta t) & \cos(\omega_{\mathrm{d}}\Delta t) - \frac{\xi\omega}{\omega_{\mathrm{d}}}\sin(\omega_{\mathrm{d}}\Delta t) \end{pmatrix} \tag{39}$$

where $\omega_{\mathrm{d}} = \sqrt{1-\xi^2}\omega$ is the damped vibration frequency.

The Taylor's series expansions of the entries of matrix $\mathbf{A}_{\mathrm{AN}}$ are given by

$$A_{\mathrm{AN}}(1,1) = 1 - \frac{\omega^2\Delta t^2}{2} + \frac{\xi}{3}\omega^3\Delta t^3 - \frac{(4\xi^2-1)}{24}\omega^4\Delta t^4 + \frac{\xi(2\xi^2-1)}{30}\omega^5\Delta t^5 - \frac{(1-12\xi^2+16\xi^4)}{720}\omega^6\Delta t^6 + \cdots \tag{40}$$

$$A_{\mathrm{AN}}(1,2) = \Delta t - \xi\omega\Delta t^2 + \frac{(4\xi^2-1)}{6}\omega^2\Delta t^3 - \frac{\xi(2\xi^2-1)}{6}\omega^3\Delta t^4 + \frac{(16\xi^4-12\xi^2+1)}{120}\omega^4\Delta t^5 - \frac{(16\xi^5-16\xi^3+3\xi)}{360}\omega^5\Delta t^6 + \cdots \tag{41}$$

$$A_{\mathrm{AN}}(2,1) = -\omega^2\Delta t + \xi\omega^3\Delta t^2 - \frac{(4\xi^2-1)}{6}\omega^4\Delta t^3 + \frac{\xi(2\xi^2-1)}{6}\omega^5\Delta t^4 - \frac{(16\xi^4-12\xi^2+1)}{120}\omega^6\Delta t^5 + \frac{(16\xi^5-16\xi^3+3\xi)}{360}\omega^7\Delta t^6 - \cdots \tag{42}$$

$$A_{\mathrm{AN}}(2,2) = 1 - 2\xi\omega\Delta t + \frac{(4\xi^2-1)}{2}\omega^2\Delta t^2 - \frac{2\xi(2\xi^2-1)}{3}\omega^3\Delta t^3 + \frac{(16\xi^4-12\xi^2+1)}{24}\omega^4\Delta t^4 - \frac{(16\xi^5-16\xi^3+3\xi)}{60}\omega^5\Delta t^5 + \frac{(64\xi^6-80\xi^4+24\xi^2-1)}{720}\omega^6\Delta t^6 - \cdots \tag{43}$$

The Taylor's series expansions of the entries of the numerical amplification matrix $\mathbf{A}$ (Eq. (17)), for the ExGA-Runge–Kutta, as a function of sub-steps n, are given by

$$A(1,1) = 1 - \frac{\omega^2\Delta t^2}{2} + \frac{\xi}{3}\omega^3\Delta t^3 - \frac{(4\xi^2-1)}{24}\omega^4\Delta t^4 + \left(1-\frac{1}{n^4}\right)\frac{\xi(2\xi^2-1)}{30}\omega^5\Delta t^5 - \left(1-\frac{6}{n^4}+\frac{5}{n^5}\right)\frac{(1-12\xi^2+16\xi^4)}{720}\omega^6\Delta t^6 + \ldots \tag{44}$$

$$A(1,2) = \Delta t - \xi\omega\Delta t^2 + \frac{(4\xi^2-1)}{6}\omega^2\Delta t^3 - \frac{\xi(2\xi^2-1)}{6}\omega^3\Delta t^4 + \left(1-\frac{1}{n^4}\right)\frac{(16\xi^4-12\xi^2+1)}{120}\omega^4\Delta t^5 - \left(1-\frac{6}{n^4}+\frac{5}{n^5}\right)\frac{(16\xi^5-16\xi^3+3\xi)}{360}\omega^5\Delta t^6 + \cdots \tag{45}$$

$$A(2,1) = -\omega^2\Delta t + \xi\omega^3\Delta t^2 - \frac{(4\xi^2-1)}{6}\omega^4\Delta t^3 + \frac{\xi(2\xi^2-1)}{6}\omega^5\Delta t^4 - \left(1-\frac{1}{n^4}\right)\frac{(16\xi^4-12\xi^2+1)}{120}\omega^6\Delta t^5 + \left(1-\frac{6}{n^4}+\frac{5}{n^5}\right)\frac{(16\xi^5-16\xi^3+3\xi)}{360}\omega^7\Delta t^6 - \cdots \tag{46}$$

$$A(2,2) = 1 - 2\xi\omega\Delta t + \frac{(4\xi^2-1)}{2}\omega^2\Delta t^2 - \frac{2\xi(2\xi^2-1)}{3}\omega^3\Delta t^3 + \frac{(16\xi^4-12\xi^2+1)}{24}\omega^4\Delta t^4 - \left(1-\frac{1}{n^4}\right)\frac{(16\xi^5-16\xi^3+3\xi)}{60}\omega^5\Delta t^5 + \left(1-\frac{6}{n^4}+\frac{5}{n^5}\right)\frac{(64\xi^6-80\xi^4+24\xi^2-1)}{720}\omega^6\Delta t^6 - \cdots \tag{47}$$

and the Taylor's series expansions of the entries of the numerical amplification matrix **A** (Eq. (37)), for the ExGAH-Central Difference, as a function of sub-steps n, are given by

$$A(1,1) = 1 - \frac{\omega^2\Delta t^2}{2} + (1-\frac{1}{n^2})\frac{\xi}{3}\omega^3\Delta t^3 - (1-\frac{1}{n^2})\frac{(4\xi^2-1)}{24}\omega^4\Delta t^4 + \cdots \tag{48}$$

$$A(1,2) = \Delta t - \xi\omega\Delta t^2 + \left(1-\frac{1}{n^2}\right)\frac{(4\xi^2-1)}{6}\omega^2\Delta t^3 - \left(1-\frac{1}{n^2}\right)\frac{\xi(2\xi^2-1)}{6}\omega^3\Delta t^4 + \cdots \tag{49}$$

$$A(2,1) = -\omega^2\Delta t + \xi\omega^3\Delta t^2 - \left(1+\frac{1}{2n^2}\right)\frac{(4\xi^2-1)}{6}\omega^4\Delta t^3 + \frac{\xi(-1-2n^2+4(2+n^2)\xi^2)}{12n^2}\omega^5\Delta t^4 - \ldots \tag{50}$$

$$A(2,2) = 1 - 2\xi\omega\Delta t + \frac{(4\xi^2-1)}{2}\omega^2\Delta t^2 - \left(1+\frac{1}{2n^2}\right)\frac{2\xi(2\xi^2-1)}{3}\omega^3\Delta t^3 + \frac{(-1+n^2-12(1+n^2)\xi^2+16(2+n^2)\xi^4)}{24n^2}\omega^4\Delta t^4 - \cdots \tag{51}$$

Comparing Eqs. (44)–(47) with Eqs. (40)–(43), it can be observed that the ExGA-Runge–Kutta is at least fourth-order accurate, i.e., the truncation errors are $O(\Delta t^5)$. It can also be inferred from Eqs. (48)–(51) that the ExGAH-Central Difference is at least second-order accurate, i.e., $O(\Delta t^3)$. Thus, the truncation error becomes smaller as the number of sub-steps n increases for both methods. It is easily seen that $\lim_{n\to\infty}\mathbf{A} = \mathbf{A}_{\mathrm{AN}}$, which demonstrates the consistency of the present method.

11. Numerical applications

In the present section, several numerical applications are presented, illustrating the potentialities of the proposed methodology. Firstly, a SDOF model is considered and, in the sequence, two MDOF acoustic models are analyzed.

11.1. Single-degree-of-freedom model

The numerical accuracy of the present method is studied by analyzing Eq. (52) below, which governs the harmonic response of a single-degree-of-freedom mechanical system:

$$\ddot{u}(t) + 2\xi\omega\dot{u}(t) + \omega^2 u(t) = 0 \tag{52}$$

with initial conditions

$$\begin{aligned} u(0) &= 1 \\ \dot{u}(0) &= 1 \end{aligned} \tag{53}$$

In the present analysis, $\omega = 2\pi$ and $\xi = 0$ are considered. The convergence rates or the order of accuracy of the methods described previously can be measured from the slope of the error curve indicated in Fig. 6, which is plotted in a double logarithmic scale. The error of the displacement, i.e., $|u(t_N) - u_N|$, is calculated at time $t_N = 1$ s, considering different numbers of time steps (N). Fig. 6 shows that the ExGA-RK, with $n = 1, 2, 5$, and the RK are fourth-order accurate while the ExGAH-CD, with $n = 1, 2, 4$, and the CD are second-order accurate. However, the error of the proposed methods decreases as n increases due to the smaller relative period error and algorithm damping ratio.

11.2. Acoustic rod

This example simulates a one-dimensional wave propagation problem in a uniform rod under an external applied load $p(t)$. The boundary conditions and the geometry of the model are depicted in Fig. 7. The rod has null initial conditions over its entire domain. The material properties and geometrical parameters considered are: $K = 3.2\times10^7$ kN/m^2, $\rho = 2000$ kg/m^3, $a = 4$ m and $b = 1$ m. The spatial domain is discretized by the second-order finite difference scheme and a central finite difference approximation is used to take into consideration

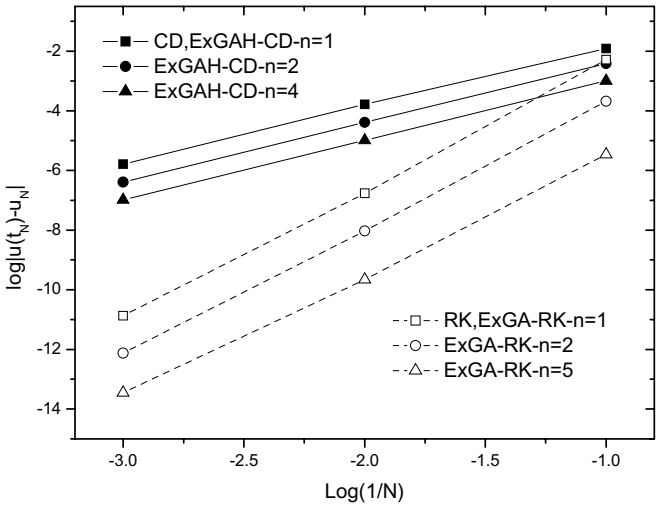

Fig. 6. Displacement rate of convergence at time $t_N = 1$ s.

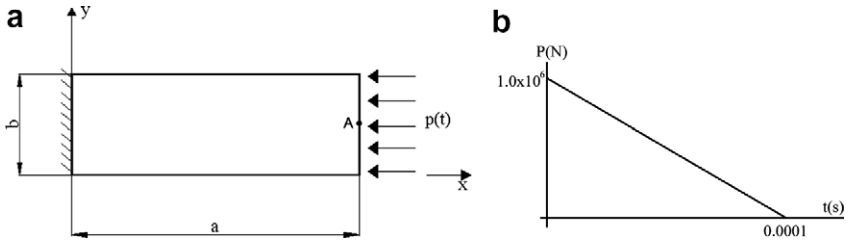

Fig. 7. Acoustic rod: (a) geometry and boundary conditions and (b) external applied load.

natural boundary conditions. The finite difference grid employed in the analysis has 1701 points ($\Delta x = \Delta y = 0.05$ m).

The displacement results at point A (a, $b/2$), provided by the RK, CD, ExGA-RK^2 and ExGA/ExGAH-CD^2 schemes, are shown in Figs. 8a,b. Accurate results are obtained considering all methods, except the ExGA-CD^2, for $\Delta t = 5.0 \times 10^{-6}$ s. This time step length was chosen so that the relation $c\Delta t \leqslant$ "element length" is obeyed, where c (medium wave propagation velocity) is given by $\sqrt{K/\rho}$. Thus, results obtained with this Δt, and the analytical solution, are taken as references to evaluate accuracy of the ExGA-RK^2 and ExGA/ExGAH-CD^2 with larger time steps.

It can be inferred from Fig. 8a that the ExGA-RK^2 method, with $n = 40$, provides good results when a large time step is considered, i.e., $\Delta t = 5.0 \times 10^{-4}$ s. This time step is one hundred times higher than the reference time step (note that the restriction $c\Delta t \leqslant$ "element length" need not to be obeyed when sub-steps are employed). Results plotted in Fig. 8a illustrate that when the rectangle rule is adopted (see expression (10)), rather than then the trapezoidal rule, less accurate results are obtained, especially for large time steps. Fig. 8b shows that accurate results are provided when the time step is increased from $\Delta t = 5.0 \times 10^{-6}$ s to $\Delta t = 2.5 \times 10^{-4}$ s, with $n = 40$, for the ExGAH-CD^2 method (the ExGA-CD^2 method blows up even for the reduced time-step $\Delta t = 5.0 \times 10^{-6}$ s, demonstrating its instability).

11.3. Membrane

The third numerical example discussed here is that of a square membrane, fixed along its boundary and submitted to an initial velocity condition $v_0(x, y) = c$ (c is the medium wave propagation velocity) applied at the gray region shown in Fig. 9a. The parameters values for this problem are: $a = 1.0$ m (square membrane

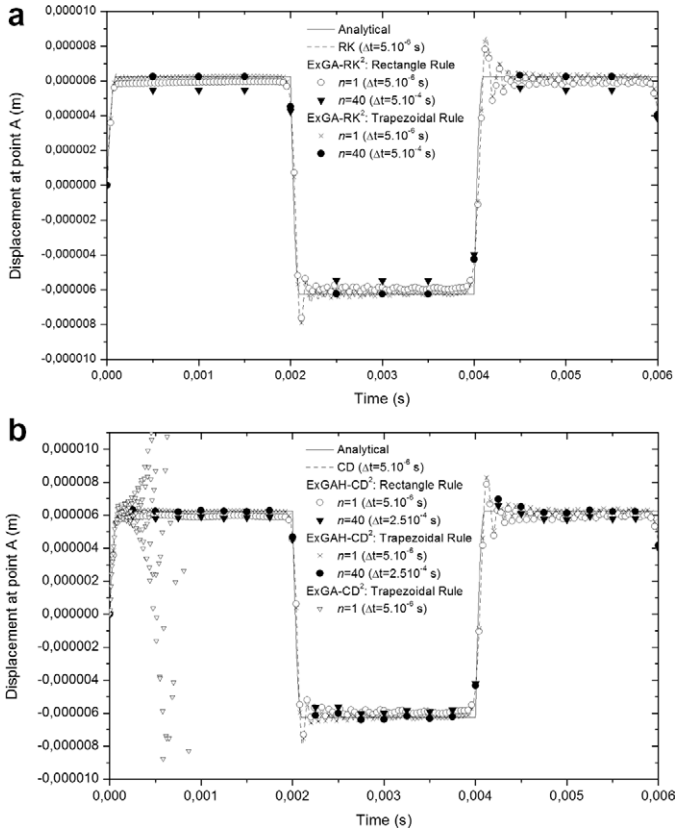

Fig. 8. Displacement time-history results at point A considering a second-order FDM and ExGA algorithms: (a) ExGA-RK^4 and (b) ExGA/ExGAH-CD^4.

length) and $c = 1.0$ m/s. The spatial domain is discretized by a fourth-order finite difference scheme, employing a regular finite difference grid of 6561 points ($\Delta h = 0.0125$ m), as shown in Fig. 9b.

The displacement time history at point A ($a/2$, $a/2$), evaluated by the ExGA-RK^4 and the ExGAH-CD^4 methods, are compared with the analytical solution [23,44], in Fig. 10. The reference time step adopted in this example is given by $\Delta t = 0.008$ s. The usual time-step estimative $c\Delta t \leqslant$ "element length", provides for the present case: $\Delta t \leqslant 0.0125$ s. In order to demonstrate the high accuracy of the two methods in focus, the time step is

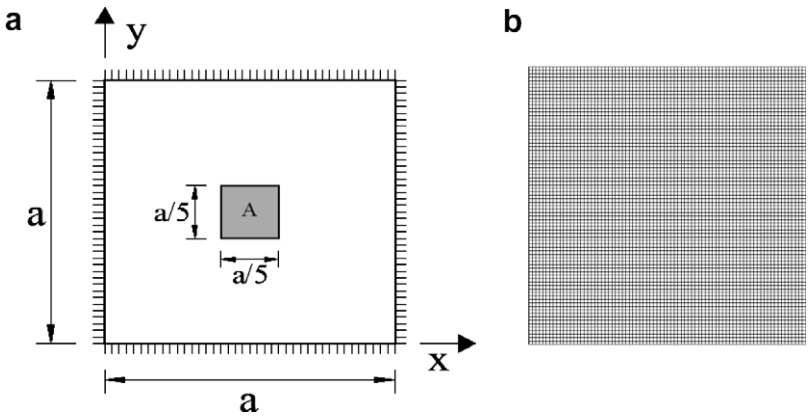

Fig. 9. Acoustic membrane: (a) geometry, boundary and initial conditions and (b) 2D finite difference grid.

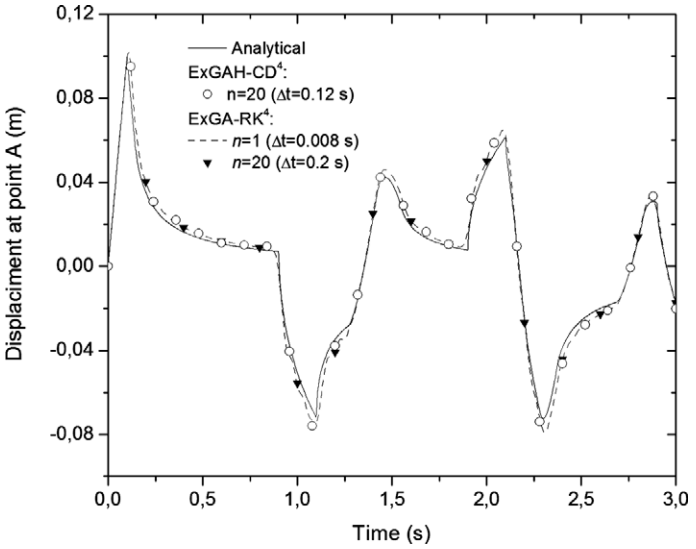

Fig. 10. Displacement time-history results at point A considering a fourth-order FDM and ExGA-RK^4 and ExGAH-CD^4 schemes.

increased up to $\Delta t = 0.2$ s, for the ExGA-RK^4 (whose stability condition allows higher time steps than the ExGAH-CD^4), and up to $\Delta t = 0.12$ s, for the ExGAH- CD^4; 20 sub-steps ($n = 20$) were employed for both cases. The numerical results are fairly good, demonstrating the high accuracy of the two schemes.

In Fig. 11, the convergence rates for the Runge–Kutta and ExGA- RK^4 schemes are analyzed trough comparison of numerical results at time $t = 2.5$ s, considering successive mesh and time step refinement (the relation $\Delta t/\Delta h$ is always kept constant). As it can be seen in Fig. 11, both methods have the same convergence rate. The ExGA-RK^4 method employed a time step five times larger than that of the standard Runge–Kutta approach, without any loss of accuracy. The ExGA-RK^4 allows time steps as large as required, with no loss of accuracy as long as more sub-steps are considered.

As it is well known, the central difference method is a very low demanding computational method. However, its main drawback is the existence of a critical time step value, which, for some engineering analyses, is too small. The present method is explicit and overcome this limitation: large time steps can be adopted without deteriorating numerical responses, once a proper number of sub-steps is considered. Thus, the method is quite

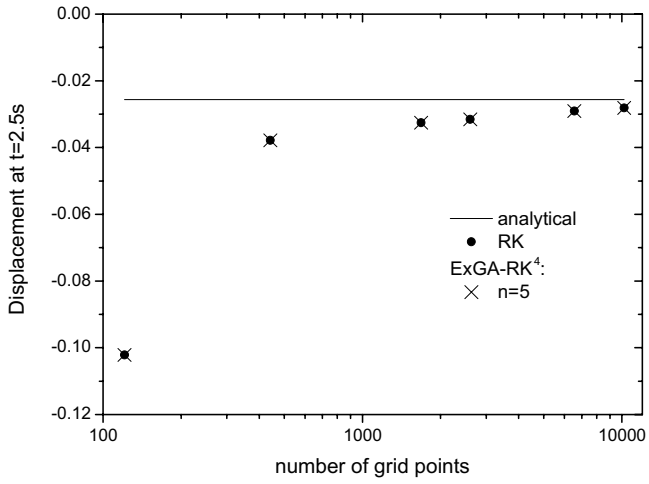

Fig. 11. Rate of convergence for the RK and ExGA-RK^4 methods ($\Delta t_{\text{ExGA-RK}^4} = 5\Delta t_{\text{RK}}$).

robust and the time-marching scheme that arises is very efficient (just few matrix–vector multiplications are necessary, where the matrices are diagonally banded). As it can be seen in Figs. 8 and 10, the ExGAH-Central Difference and ExGA-Runge–Kutta schemes provide good results considering large time steps, which are prohibitive for the Central Difference and Runge–Kutta methods.

A good estimative of the ratio between the number of arithmetic operations per time step of the matrix–vector products required by the ExGAH and the back substitution operations of implicit FEM algorithms is given by the parameter $\alpha = \theta \frac{N_x}{N_f} \frac{\Delta t_f}{\Delta t_x}$, where Δt_f and Δt_x are, respectively, the time steps of FEM and ExGAH analyses. N_f is the bandwidth of the FEM effective system matrix and N_x is the ratio between the total number of non-null coefficients of the ExGAH **G** (or **H**) matrix, divided by the total number of equations. N_x increases and so does the CPU time, as the number of sub-steps of the ExGAH algorithm increases; however, more sub-steps permit larger Δt_x, and thus, additional cost reduction. If a FEM algorithm which works with fix bandwidth is employed, α will be in most cases much less than 1 for complex large scale problems and higher than 1 for simple applications. Programs that optimize the bandwidth and skyline procedures can improve the performance of FEM implicit algorithms and in some cases can make the CPU time close (or even lower) than that of the ExGAH approach.

12. Conclusions

The present paper describes a new family of explicit time integration methods called ExGA, which are based on numerical calculation of Green's matrices. Standard explicit algorithms, such as central differences, Runge–Kutta and generalized-α, may have a too short critical time step for a great range of problems, in which case, implicit schemes may be required. The new algorithms presented here are explicit but have no time-step restriction for all practical purposes: a time-step one hundred times greater than that recommended for standard central differences time-marching schemes was considered with no loss either of accuracy or stability. In fact, the algorithm described here permits controlling its critical time step when sub-steps are used: the more sub-steps one uses, the larger the critical time step. Moreover, employing sub-steps leads to quite low artificial damping or period distortion.

The paper also presented the ExGAH approach, under the same concepts of the ExGA. Thus, the ExGAH became quite flexible, being easy to establish the corresponding expressions to a great range of physical–mathematical models. The development presented here shows also that it is straightforward to use any numerical method to account for spatial discretization, as well as any time marching scheme to compute Green's and unit step functions and their time derivative matrices.

Not only the present explicit method can be considered unconditionally stable for all practical purposes, but also, since it can march with large time steps, it is a very attractive tool considering long period problems. In this case, the time marching process consists of only few matrix–vector multiplications (the matrices being diagonally banded), whereas in standard unconditionally stable methodologies (implicit approaches), one system of equations must be dealt with at each time step and the time step must be much smaller in order to keep accuracy, requiring a larger amount of time marching steps and operations.

References

[1] L.A. Souza, J.A.M. Carrer, C.J. Martins, A fourth order finite difference method applied to elastodynamics: finite element and boundary element formulations, Structural Engineering and Mechanics 17 (2004) 735–749.
[2] G.M. Hulbert, J. Chung, Explicit time integration algorithms for structural dynamics with optimal numerical dissipation, Computer Methods in Applied Mechanics and Engineering 137 (1996) 175–188.
[3] J. Chung, J.M. Lee, A new family of explicit time integration methods for linear and non-linear structural dynamics, International Journal for Numerical Methods in Engineering 37 (1994) 3961–3976.
[4] G.D. Hahn, A modified Euler method for dynamic analysis, International Journal for Numerical Methods in Engineering 32 (1991) 943–955.
[5] C. Hoff, R.L. Taylor, Higher derivative explicit one step methods for non-linear dynamic problems. Part I: design and theory, International Journal for Numerical Methods in Engineering 29 (1990) 275–290.
[6] K.K. Tamma, R.R. Namburu, A robust self-starting explicit computational methodology for structural dynamic applications: architecture and representations, International Journal for Numerical Methods in Engineering 29 (1990) 1441–1454.

[7] J. Chung, J.M. Hulbert, A time integration method for structural dynamics with improved numerical dissipation: the generalized α-method, Journal of Applied Mechanics 30 (1993) 371–375.
[8] H.M. Hilber, T.J.R. Hughes, R.L. Taylor, Improved numerical dissipation for time integration algorithms in structural dynamics, Earthquake Engineering and Structural Dynamics 5 (1977) 283–292.
[9] E.L. Wilson, A Computer Program for Dynamic Stress Analysis of Underground Structures, SESM, University of California, Berkeley, 1968.
[10] N.M. Newmark, A method of computation for structural dynamics, Journal Engineering Mechanics Division, ASCE 85 (1959) 67–94.
[11] J.C. Houbolt, A recurrence matrix solution for the dynamic response of elastic aircraft, Journal of the Aeronautical Sciences 17 (1950) 540–550.
[12] K.K. Tamma, X. Zhou, D. Sha, The time dimension: a theory towards the evolution, classification, characterization and design of computational algorithms for transient dynamic applications, Archives of Computational Methods in Engineering 7 (2000) 67–286.
[13] T.C. Fung, A precise time-step integration method by step-response and impulsive-response matrices for dynamic problems, International Journal for Numerical Methods in Engineering 40 (1997) 4501–4527.
[14] W.J.T. Daniel, Analysis and implementation of a new constant acceleration subcycling algorithm, International Journal for Numerical Methods in Engineering 40 (1997) 2841–2855.
[15] P. Smolinski, Subcycling integration with non-integer time steps for structural dynamics problems, Computers & Structures 59 (1996) 273–281.
[16] M. Mancuso, F. Ubertini, A methodology for the generation of low-cost higher-order methods for linear dynamics, International Journal for Numerical Methods in Engineering 56 (2003) 1883–1912.
[17] T.C. Fung, Unconditionally stable higher-order Newmark methods by sub-stepping procedure, Computer Methods in Applied Mechanics and Engineering 147 (1997) 61–84.
[18] T.C. Fung, Higher-order accurate time-step-integration algorithms by post-integration techniques, International Journal for Numerical Methods in Engineering 53 (2002) 1175–1193.
[19] A. Safjan, J.T. Oden, High-order Taylor–Galerkin and adaptive hp methods for second-order hyperbolic systems: application to elastodynamics, Computer Methods in Applied Mechanics and Engineering 103 (1993) 187–230.
[20] A. Safjan, J.T. Oden, High-order Taylor–Galerkin methods for linear hyperbolic systems, Journal of Computational Physics 120 (1995) 206–230.
[21] J. Kujawski, R.H. Gallagher, A family of higher-order explicit algorithms for the transient dynamic analysis, Society for Computer Simulation, Transactions 1 (1984) 155–166.
[22] G.M. Hulbert, I. Jang, Automatic time step control algorithms for structural dynamics, Computer Methods in Applied Mechanics and Engineering 126 (1995) 155–178.
[23] W.J. Mansur, A Time-stepping Technique to Solve Wave Propagation Problems using the Boundary Element Method, Ph.D. Thesis, University of Southampton, England, 1983.
[24] L.C. Wrobel, Potential and Viscous Flow Problems using the Boundary Element Method, Ph.D. Thesis, University of Southampton, England, 1981.
[25] D. Soares Jr., W.J. Mansur, A time domain FEM approach based on implicit Green's functions for nonlinear dynamic analysis, International Journal for Numerical Methods in Engineering 62 (2005) 664–681.
[26] K.K. Tamma, D. Sha, X. Zhou, Time discretized operators. Part1: towards the theoretical design of a new generation of a generalized family of unconditionally stable implicit and explicit representations of arbitrary order for computational dynamics, Computer Methods in Applied Mechanics and Engineering 192 (2003) 257–290.
[27] X. Zhou, K.K. Tamma, A new unified theory underlying time dependent linear first-order systems: a prelude to algorithms by design, International Journal for Numerical Methods in Engineering 60 (2004) 1699–1740.
[28] W.J. Mansur, Explicit Algorithms based on Green's Functions (ExGA) to Integrate the Equations of Motion, Lecture at Civil Engineering Department, COPPE-UFRJ, January 2005 (in Portuguese).
[29] F. Loureiro, A Time Marching Procedure based on Green's Functions Computed by the FEM, Graduation Report, Mechanical Engineering Department, COPPE-UFRJ, August 2006 (in Portuguese).
[30] W.X. Zhong, F.W. Williams, A precise time step integration method, Journal of Mechanical Engineering Science 208 (1994) 427–450.
[31] W. Zhong, Z. Jianing, X.X. Zhong, On a new time integration method for solving time dependent partial differential equations, Computer Methods in Applied Mechanics and Engineering 130 (1996) 163–168.
[32] T.J.R. Hughes, The Finite Element Method, Dover Publications INC., New York, 1987.
[33] K.J. Bathe, Finite Element Procedures, Prentice-Hall, Englewood Cliffs, NJ, 1996.
[34] M. Paz, Structural Dynamics – Theory and Computation, fourth ed., Chapman and Hall, New York, 1997.
[35] W. Weaver Jr., P.R. Johnston, Structural Dynamics by Finite Elements, Prentice-Hall, Englewood Cliffs, NJ, 1987.
[36] O.C. Zienkiewicz, R.L. Taylor, J.Z. Zhu, The Finite Element Method its Basis & Fundamentals, sixth ed., Butterworth-Heinemann, Oxford, 2005.
[37] R.W. Clough, J. Penzien, Dynamics of Structures, second ed., McGraw-Hill, New York, 1993.
[38] S.S. Rao, Mechanical Vibrations, Addison-Wesley Publishing Company, New York, 1995.
[39] W.T. Thomson, M.D. Dahleh, Theory of Vibration with Applications, fifth ed., Prentice-Hall, Englewood Cliffs, NJ, 1993.
[40] D. Sha, X. Chen, K.K. Tamma, Virtual-pulse time integral methodology: a new approach for computational dynamics. Part 1. Theory for linear structural dynamics, Finite Elements in Analysis and Design 20 (1995) 179–194.

[41] K.K. Tamma, X. Chen, D. Sha, An overview of recent advances and evaluation of the virtual-pulse (vip) time-integral methodology for general structural dynamics problems: computational issues and implementation aspects, International Journal for Numerical Methods in Engineering 39 (1996) 1955–1977.
[42] D. Soares Jr., W.J. Mansur, An efficient time/frequency domain algorithm for modal analysis of non-linear models discretized by the FEM, Computer Methods in Applied Mechanics and Engineering 192 (2003) 3731–3745.
[43] B. Yang, Stress, Strain and Structural Dynamics, Elsevier Academic Press, 2005.
[44] J.A.M. Carrer, W.J. Mansur, Time-domain BEM analysis for the 2D scalar wave equation: initial conditions contributions to space and time derivatives, International Journal for Numerical Methods in Engineering 39 (1997) 2188–2469.
[45] P.M. Morse, H. Feshbach, Methods of Theoretical physics, McGraw-Hill, New York, Toronto and London, 1953.
[46] M. Géradin, D. Rixen, Mechanical Vibrations Theory and Application to Structural Dynamics, John Wiley & Sons, Paris, 1994.